Check for updates

The hidden features of fullerene rotation in the crystal lattice†

Yajuan Hao,[b,c] Yaofeng Wang,[b] Christian G. Feiler,[d] Manfred S. Weiss, [iD] [d]
Alexey A. Popov [iD] *[b] and Fupin Liu [iD] *[a]

Rotational dynamics in the crystal lattice is a characteristic attribute of fullerenes caused by their spherical shape. It lies in the background of various multifaceted phenomena, ranging from severe disorder, often hampering diffraction studies of fullerenes, to rotational order–disorder transitions or controlled switching of molecular orientations in nanoscale devices. Understanding these dynamics and their real-space presentation still remains a complex problem, especially for endohedral metallofullerenes, as their encapsulated species may show additional rotational degrees of freedom. In this work, we used variable-temperature single-crystal X-ray diffraction (VT SC-XRD) to elaborate on the phase transition in $Sc_3N@C_{70}$ crystals caused by the rotation of fullerene molecules. Snapshots of the molecular rotation taken with 10 K steps in a broad temperature range provided in-depth description of the process and revealed details usually overlooked by SC-XRD studies of metallofullerenes. In particular, analysis of thermal ellipsoids at various temperatures allowed to distinguish hidden static disorder from apparent dynamic disorder caused by thermal motion. The results mark a leap to the fundamental understanding of the unique metallofullerene structural characters, paving the way to control fullerene movement state in single molecule devices built from fullerenes.

Introduction

Endohedral metallofullerenes (EMFs) are molecules with metal ions encapsulated inside fullerene cages. The coordination of metal ions to the inner wall of carbon cage with its extended π-system results in unique physicochemical properties, promising wide potential in biomedicine, energy, and emerging molecular devices.[1–7] The coordination between encapsulated metal ions and the fullerene cage is fundamentally important to understand the structure–property relations.[6,7] As one of the most interesting properties of EMFs, the intrinsic dynamics of metallofullerene molecules in solid state is still poorly understood, in strong contrast to the deep understanding of structural versatility of metallofullerenes.[8–20]

[a]Jiangsu Key Laboratory of New Power Batteries, School of Chemistry and Materials Science, Nanjing Normal University, Nanjing 210023, China. E-mail: liu_fupin@nnu.edu.cn
[b]Leibniz Institute for Solid State and Materials Research (IFW Dresden), Helmholtzstr. 20, 01069 Dresden, Germany. E-mail: a.popov@ifw-dresden.de
[c]School of Electrical and Mechanical Engineering, Pingdingshan University, Pingdingshan 467000, China
[d]Macromolecular Crystallography (BESSY-MX), Elektronenspeicherring BESSY II, Helmholtz Zentrum Berlin, Albert-Einstein-Str. 15, 12489 Berlin, Germany
†Electronic supplementary information (ESI) available: Details of single crystal X-ray diffraction data. CCDC 2362043–2362055. For ESI and crystallographic data in CIF or other electronic format see DOI: https://doi.org/10.1039/d4qi01562b
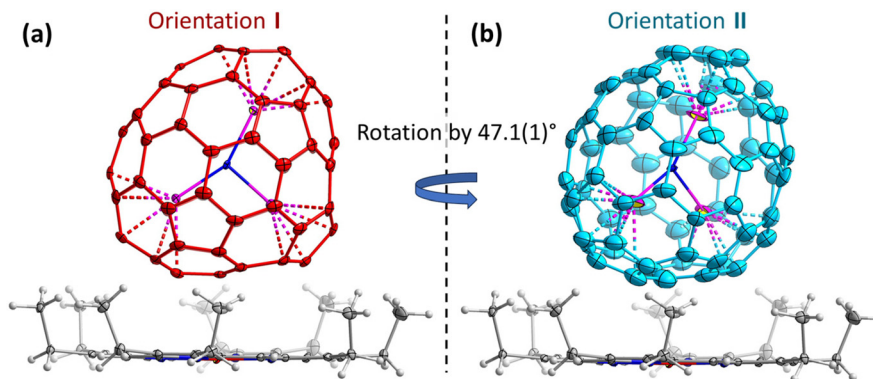
A strategy to tackle this challenge is to observe the metal movement driven by temperature with variable temperature single crystal X-ray diffraction (VT SC-XRD). A few notable examples of this strategy include observing the standing still La/Gd ions in adamantylidene-derivatized C_{82} cage until 293 K;[21,22] standing still of two La ions in adamantylidene-derivatized C_{80} cage till 273 K;[23] jumping of Yb ion in C_{80} cage;[24] moving of M_3N (M_3 = Ho_2Lu, Lu_3, Dy_2Sc, and Sc_3) in C_{80} cage;[25–28] rotation of Dy_2 in benzyl-derivatized C_{80};[29] moving of UN in C_{82};[30] and rotation of the whole $Sc_3N@C_{70}$ molecule with $C_{2v}(7854)$ carbon cage[31] in the crystal lattice (Fig. 1 and Fig. S1 in the ESI†).[32] The current state-of-the-art variable temperature single crystal X-ray diffraction studies captured the movement information with coarse precision, but the detailed information on the movement in high precision is still missing, although such information is pivotal to evaluate the intra/inter-molecular interactions. The strong coordination between Sc ions and the adjacent pentagon pairs of C_{70} in $Sc_3N@C_{70}$ effectively excludes the degree of freedom for metal ions movement relative to the fullerene cage in the studied temperature range,[33–35] thus disentangles the complicated simultaneous movements of metal ions and fullerene cage in the crystal lattice. Therefore, this crystal exemplifies an ideal system to study the details of metallofullerene movement in the crystal lattice. In this work, we took a lot of snapshots for fullerene rotation with VT SC-XRD, to

This journal is © the Partner Organisations 2024

Inorg. Chem. Front., 2024, **11**, 6343–6349 | **6343**

Fig. 1 Coordination of $Sc_3N@C_{70}$ molecule to the NiOEP in two orientations present in different ratio in all crystals of $Sc_3N@C_{70} \cdot NiOEP \cdot 0.5$ $(C_6H_6) \cdot C_7H_8$ studied in this work. The shown structures are for crystal **2** at $T = 50$ K, the major orientation **I** has occupancy of 79%, the minor orientation **II** has occupancy of 21%. Color code: grey for C in NiOEP, blue for N, white for H, magenta for Sc, red and cyan for C in fullerene cages. The probability of thermal ellipsoids was set to 30%.

unravel the hidden details of fullerene movement in the crystal lattice.

Results and discussion

The crystals $Sc_3N@C_{70} \cdot NiOEP \cdot 0.5(C_6H_6) \cdot C_7H_8$ were grown by layering the toluene solution of $Sc_3N@C_{70}$ on the benzene solution of nickel octaethylporphyrin (NiOEP).[32,36] Analysis of the VT-SC-XRD data in this work is based on the studies of three crystals from two growth batches. Crystal **1** was studied in ref. 32 at 100, 160, and 220 K and revealed first indication of the phase transition below 160 K. Two orientations of the fullerene molecule present at occupancy ratio of 0.76/0.24 at 100 K, attained an equal occupancy at 160 K, while the crystal space group changed from $P2_1/c$ to $C2/m$. In the following discussion, the main/minor orientations in the low-temperature crystals are denoted as orientation **I**/**II** (Fig. 1). Since the crystal had small solvent molecules (toluene and benzene) tending to slowly escape from the lattice, more recent attempts to perform detailed VT-SC-XRD study of crystal **1** showed that it degraded over time of ~6 months. New batch of crystals was therefore grown in this work reproducing the growth conditions from ref. 32. The composition and a structure of new crystals closely reproduced those of crystal **1**, aside from the small variation of the solvent content as will be discussed in more details below. One crystal from the new batch (crystal **2** hereafter) was studied at temperatures below 100 K applying cooling with He stream, while another one (crystal **3**) was measured with small temperature steps above 100 K using cooling with N_2 stream. X-ray diffraction data collection was carried out at the BESSY II storage ring (BL14.2 and BL14.3, Berlin-Adlershof, Germany).[37] XDSAPP2.0 suite was employed for data processing.[38,39] The structure was solved by direct methods and refined by SHELXL-2018.[40] Hydrogen atoms were added geometrically and refined with a riding model. The crystal data are presented in Tables S1–S3 in the ESI.†

The driving force for the phase transition in $Sc_3N@C_{70} \cdot NiOEP$ crystals around 160 K is the slightly higher thermodynamic stability of the state, in which molecules in a certain orientation are surrounded by molecules in the same orientation.[31] Above the phase transition temperature, thermally-induced re-orientational motion equalizes two orientations, while below 160 K, one of the orientations gains higher occupancy leading to the lower crystallographic symmetry. Therefore, the phase transition can be followed by monitoring the ratio of the occupancies with temperature as shown in Fig. 2a. In crystal **1**, orientations **I** and **II** show the 0.5/0.5 ratio at 220 and 160 K, but change to 0.76/0.24 at 100 K. The detailed investigation of site occupancies in crystal **3** between 100 and 190 K showed that the ratio gradually changes from 0.5/0.5 at 170–190 K, to 0.52/0.48 at 160 K, and all the way to 0.79/0.21 at 100 K (see Fig. 1 and S2, Table S4 in the ESI for more details†). Reorientation of $Sc_3N@C_{70}$ is accompanied by a switching of coordinating NiOEP molecule between two positions, related by a translational movement and shifted from each other by less than 0.6 Å (see Fig. S3 and Table S4 in the ESI for details†). To analyze if further redistribution between orientations **I** and **II** is possible below 100 K, crystal **2** was studied with He cooling. The trend towards larger difference between occupancies at lower temperature was observed here as well, but the changes between 80 K (0.74/0.26) and 50 K (0.79/0.21) appeared less pronounced than at 100–170 K. Thus, the low-temperature ratio between two orientations seems to saturate at 0.8/0.2.

Notably, different crystals show certain variation in **I**/**II** occupancy ratio when compared at the same temperatures. For instance, equal occupancies of **I** and **II** are found at 160 K in crystal **1** but at 170 K in crystal **2**, and a similar occupancy of 0.76/0.24 and 0.75/0.25 was observed for crystals **1** at 100 K, and **2** at 110 K, respectively, showing that there is a systematic shift of ~10 K between the two crystals. Likewise, the ratio of 0.74/0.26 determined for crystal **2** at 80 K is similar to the 0.75/0.25 ratio in crystal **3** at 110 K. One of the plausible reasons is
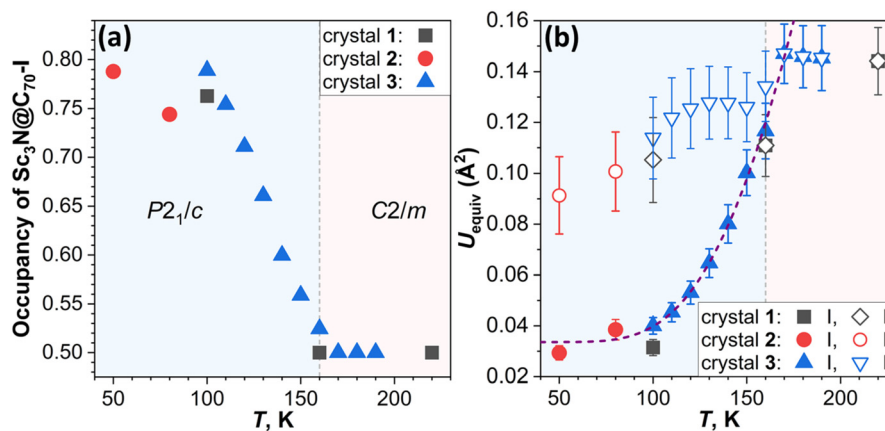
6344 | *Inorg. Chem. Front.*, 2024, **11**, 6343–6349

This journal is © the Partner Organisations 2024

Fig. 2 (a) The site occupancy of $Sc_3N@C_{70}$ orientation **I** *vs.* temperature. (b) Temperature dependence of the average equivalent atom displacement parameter (U_{equiv}) of the carbon cage in two orientations of the $Sc_3N@C_{70}$ molecule (**I** and **II**), error bars denote standard deviations within the sets of 70 carbons; dashed purple line is the fit of the data for orientation **I** in crystal **3** between 100 and 170 K by a function $a + bc\text{th}(h\nu/2kT)$.

the variation of the crystal quality between these three crystals. To verify this possibility, we refined the structures with flexible site occupancies for solvent molecules and obtained 0.898 $(C_7H_8)/0.479(C_6H_6)$ for crystal **1** at 100 K, $0.915(C_7H_8)/0.47$ (C_6H_6) for crystal **2** at 50 K, and $0.930(C_7H_8)/0.482(C_6H_6)$ for crystal **3** at 100 K (see Tables S1–S3 in the ESI for details†). The ideally perfect solvent composition used in the refinement is $C_7H_8/0.5(C_6H_6)$. As uncertainties in occupancy determination is less than 0.009, the deviations from 1.0/0.5 are statistically significant and can be attributed to the escape of solvent molecules from the lattice, leaving behind imperfections in the crystal. Crystal **3** has the highest solvent occupancy, indicating the highest perfection of the structure. Since the solvent-fullerene interaction effectively hinders the fullerene rotation,[28] the higher perfection in terms of the solvate content leads to the higher phase transition temperature. This finding highlights the importance of using fresh crystals in SC-XRD studies of fullerene solvates. Another factor to be considered is that molecular re-orientation requires overcoming of an energy barrier and can therefore become more hindered at low temperatures.[41] This makes the ratio between orientation **I** and **II** dependent on the cooling rate and can eventually result in the freezing of the **I/II** ratio when thermal energy becomes insufficient to overcome the barrier.

Observing the crystal structures with temperature intervals of 10 K results in the detailed description of the phase transition process. Fig. 3 presents the structures of crystal **3** measured at temperatures ranging from 100 to 170 K. Two overlapping orientations of $Sc_3N@C_{70}$ are equally populated at 170–190 K, with the $C2/m$ crystal space group. When temperature decreases below 170 K, part of $Sc_3N@C_{70}$ molecules rotates from orientation **II** to orientation **I**, thus resulting in their unequal populations and the loss of the mirror symmetry and reducing the crystal space group to $P2_1/c$. Remarkably, thermal ellipsoids of the two molecular orientations exhibit very different temperature evolution. At 100 K, the size of thermal ellipsoids in **I** is several times smaller than in orien-

tation **II**. But then, ellipsoids in orientation **II** barely change between 100 and 170 K, whereas the size of ellipsoids in orientation **I** increases four-fold in the same temperature range (Fig. 3). Numerically, this phenomenon is visualized in Fig. 4 using equivalent atom displacement parameters (ADPs, U_{equiv}). While ADPs for orientation **I** plotted in the upper panel show pronounced temperature dependence, a much weaker temperature variation and a larger scattering of ADPs are seen for orientation **II** in the lower panel. Temperature dependence of ADPs averaged over carbon cage in two orientations further substantiates this observation (Fig. 2b).

Temperature dependence of ADPs is associated with the variation of vibrational amplitudes, which in harmonic approximation scale with the temperature as $u_i^2 \sim \text{cth}(h\nu_i/2kT)$. Indeed, the growth of averaged cage ADPs in orientation **I** between 100 and 170 K is well described by $\text{cth}(h\nu/2kT)$ with ν of 480 ± 30 cm^{-1} (Fig. 2b). This frequency should not be understood as that of one particular mode but rather as a cumulative contribution of many vibrations. Thus, ADPs in orientation **I** show temperature variation typical for vibrational motions. The increased size of ellipsoids and the lack of their temperature dependence in orientation **II** indicate that the size of ellipsoids is likely to be determined by the static disorder. Presumably, the orientation **II** in fact contains several sub-orientations with small orientational differences, which cannot be resolved in a routine SC-XRD analysis. Thus, different temperature dependence of thermal ellipsoids allows VT SC-XRD analysis to distinguish two types of disorder coexisting in the crystal.

The concrete information observed with single crystal X-ray diffraction allows one to specifically check the chemical environment of the interested target. Fig. 5 shows the environment of $Sc_3N@C_{70}$ in the crystal lattice, presenting four nearby solvent molecules, of which one toluene molecule interacts with fullerene cage through π–π interaction, while the other two toluene and one benzene molecules interact with fullerene cage through C–H···π interaction. Fig. S4 and S5 in the ESI†

This journal is © the Partner Organisations 2024

Inorg. Chem. Front., 2024, **11**, 6343–6349 | **6345**
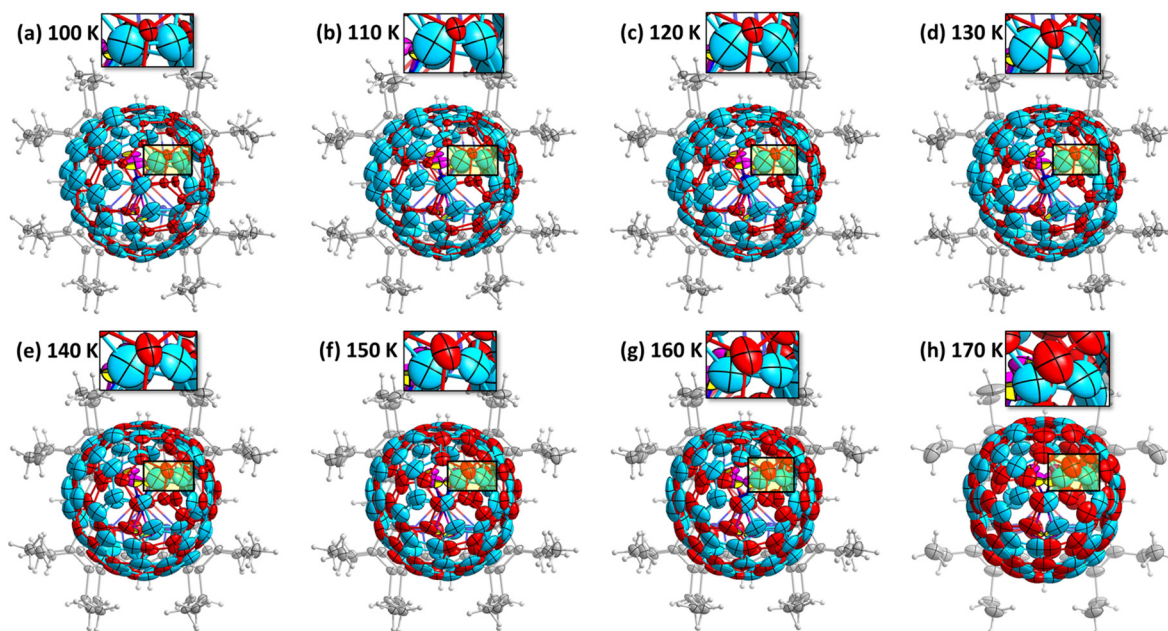
Fig. 3 Structures of crystal **3** measured at 100 K (a), 110 K (b), 120 K (c), 130 K (d), 140 K (e), 150 K (f), 160 K (g), and 170 K (h). The solvent molecules were omitted for clarity. The probability of thermal ellipsoids was set to 30%. The two orientations of C_{70} were highlighted with red for **I**, and cyan for **II**. The marked fragment was zoomed in to highlight the changes of the thermal ellipsoids with temperature. Color code: grey for C in NiOEP, blue for N, white for H, magenta for Sc.
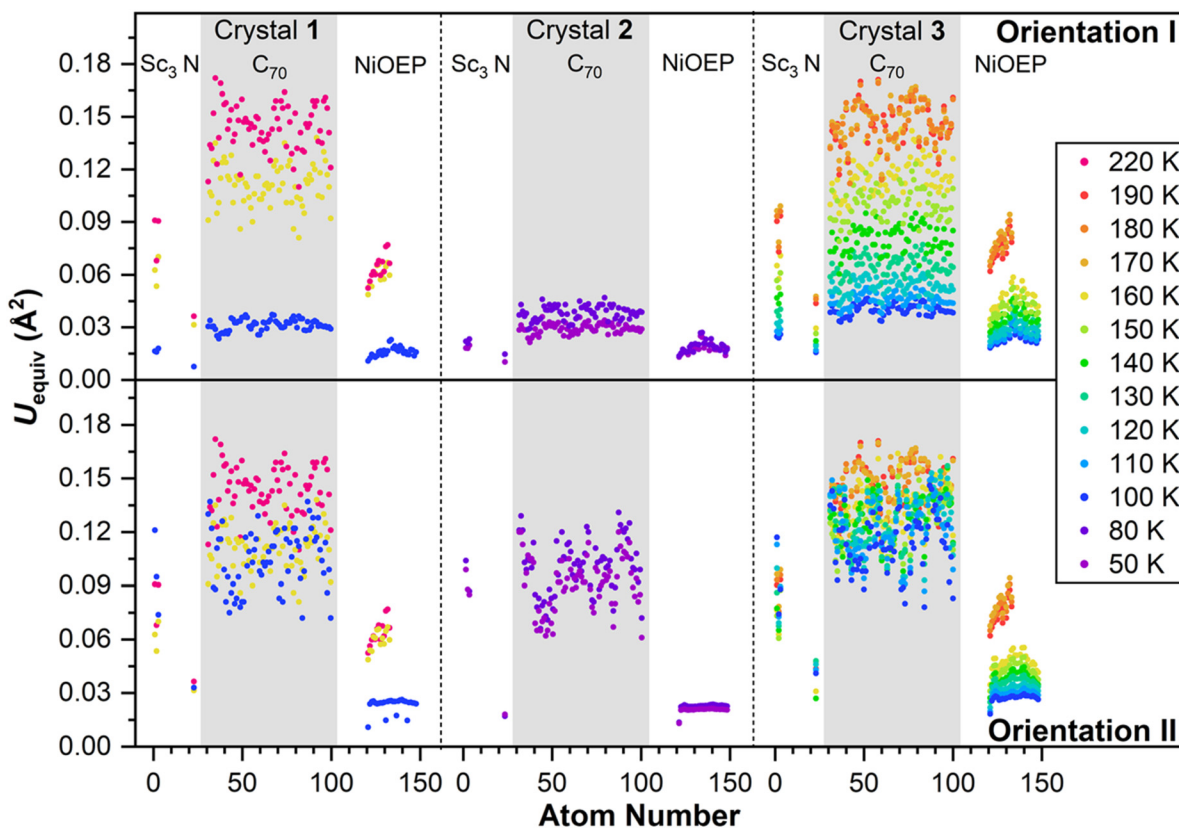

Fig. 4 The equivalent atom displacement parameters (ADPs, U_{equiv}) of $Sc_3N@C_{70}$ and NiOEP and their variation with temperature for orientation **I** (top panel) and orientation **II** (bottom panel). To guide the eye, the range of atom numbers corresponding to the carbon cage is shaded.
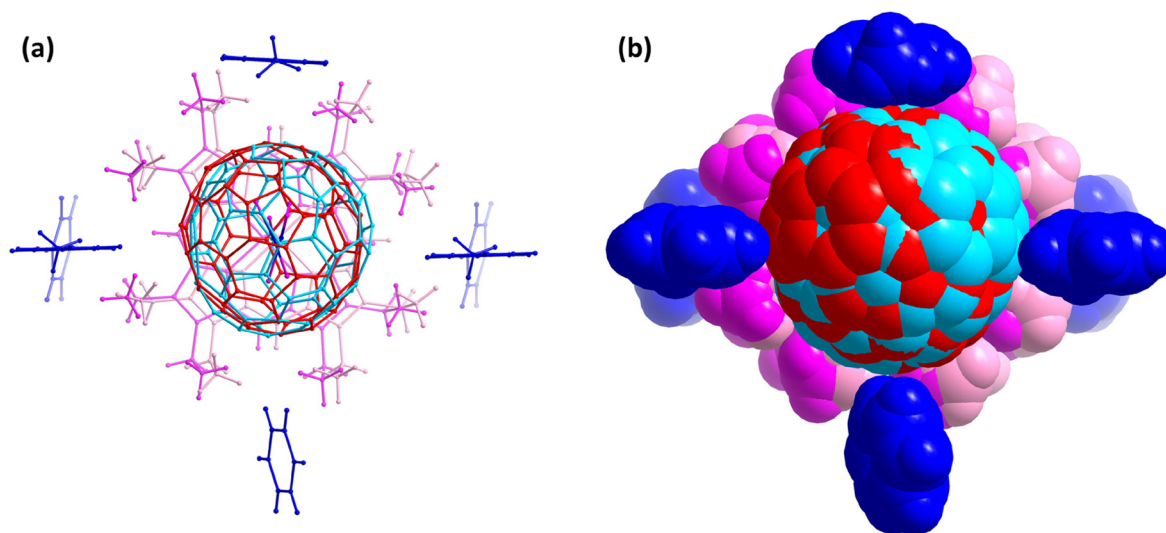
Fig. 5 The structure of crystal **3** at 100 K viewed perpendicular to the NiOEP plane. Both Ball-stick model (a) and space-filling model (b) are shown to highlight the environment of $Sc_3N@C_{70}$. Color codes: red/cyan for fullerene orientations I/II, pink/rose for NiOEP orientations I/II, blue for benzene/toluene molecules interacting with the fullerene cage and NiOEP.

highlights the solvent molecules interacting with NiOEP. Disorder usually poses higher uncertainty on the observed structural parameters, Table S5 in the ESI† presents the Sc–N bond lengths at variable temperatures. As the axis of fullerene rotation locates near the N position, the Sc–N bond lengths are weakly affected by the rotation and present rather low uncertainty at variable temperatures.

Conclusion

In conclusion, detailed information of fullerene $Sc_3N@C_{70}$ rotation in the crystal lattice unravels two unprecedentedly important phenomena: first, the subtle variation of the solvent content affects the phase transition temperature; second, co-existence of thermal vibrational motion and static disorder in one crystal was visualized and clearly distinguished through the highly contrasting behavior of thermal ellipsoids. The results lay concrete evidence on the detailed information of fullerene movement in the crystal lattice, paving the way to control the fullerene movement state in single molecule device.

Data availability

Crystallographic data for crystals of $Sc_3N@C_{70}$ measured at different temperatures has been deposited at the CCDC under numbers 2362043–2362055† and can be obtained from **https://www.ccdc.cam.ac.uk/structures/**

Conflicts of interest

There is no conflict of interest to report.

Acknowledgements

References

1 A. A. Popov, S. Yang and L. Dunsch, Endohedral Fullerenes, *Chem. Rev.*, 2013, **113**, 5989–6113.

2 X. Lu, L. Feng, T. Akasaka and S. Nagase, Current status and future developments of endohedral metallofullerenes, *Chem. Soc. Rev.*, 2012, **41**, 7723–7760.

3 F. Liu, L. Spree, D. S. Krylov, G. Velkos, S. M. Avdoshenko and A. A. Popov, Single-Electron Lanthanide-Lanthanide Bonds Inside Fullerenes toward Robust Redox-Active Molecular Magnets, *Acc. Chem. Res.*, 2019, **52**, 2981–2993.

4 L. Bao, P. Peng and X. Lu, Bonding inside and outside Fullerene Cages, *Acc. Chem. Res.*, 2018, **51**, 810–815.

5 S. Yang, T. Wei and F. Jin, When metal clusters meet carbon cages: endohedral clusterfullerenes, *Chem. Soc. Rev.*, 2017, **46**, 5005–5058.

6 K. Zhang, C. Wang, M. Zhang, Z. Bai, F.-F. Xie, Y.-Z. Tan, Y. Guo, K.-J. Hu, L. Cao, S. Zhang, X. Tu, D. Pan, L. Kang, J. Chen, P. Wu, X. Wang, J. Wang, J. Liu, Y. Song, G. Wang, F. Song, W. Ji, S.-Y. Xie, S.-F. Shi, M. A. Reed and B. Wang, A $Gd@C_{82}$ single-molecule electret, *Nat. Nanotechnol.*, 2020, **15**, 1019–1024.

This journal is © the Partner Organisations 2024

Inorg. Chem. Front., 2024, **11**, 6343–6349 | **6347**

7 J. Li, S. Hou, Y.-R. Yao, C. Zhang, Q. Wu, H.-C. Wang, H. Zhang, X. Liu, C. Tang, M. Wei, W. Xu, Y. Wang, J. Zheng, Z. Pan, L. Kang, J. Liu, J. Shi, Y. Yang, C. J. Lambert, S.-Y. Xie and W. Hong, Room-temperature logic-in-memory operations in single-metallofullerene devices, *Nat. Mater.*, 2022, **21**, 917–923.

8 Y.-R. Yao, X.-M. Shi, S.-Y. Zheng, Z.-C. Chen, S.-Y. Xie, R.-B. Huang and L.-S. Zheng, Atomically Precise Insights into Metal-Metal Bond by Comparable Endo-Units of Sc_2 and Sc_2C_2, *CCS Chem.*, 2021, **3**, 294–302.

9 Y. Yan, L. Abella, R. Sun, Y.-H. Fang, Y. Roselló, Y. Shen, M. Jin, A. Rodríguez-Fortea, C. de Graaf, Q. Meng, Y.-R. Yao, L. Echegoyen, B.-W. Wang, S. Gao, J. M. Poblet and N. Chen, Actinide-lanthanide single electron metal-metal bond formed in mixed-valence di-metallofullerenes, *Nat. Commun.*, 2023, **14**, 6637.

10 W. Xiang, Z. Hu, J. Xin, H. Jin, Z. Jiang, X. Han, M. Chen, Y.-R. Yao and S. Yang, Steering Single-Electron Metal–Metal Bonds and Hyperfine Coupling between a Transition Metal-Lanthanide Heteronuclear Bimetal Confined in Carbon Cages, *J. Am. Chem. Soc.*, 2023, **145**, 22599–22608.

11 W. Yang, G. Velkos, M. Rosenkranz, S. Schiemenz, F. Liu and A. A. Popov, Nd–Nd Bond in I_h and D_{5h} Cage Isomers of $Nd_2@C_{80}$ Stabilized by Electrophilic CF_3 Addition, *Adv. Sci.*, 2024, **11**, 2305190.

12 W. Yang, M. Rosenkranz, G. Velkos, F. Ziegs, V. Dubrovin, S. Schiemenz, L. Spree, M. F. de Souza Barbosa, C. Guillemard, S. M. Valvidares, B. Büchner, F. Liu, S. Avdoshenko and A. A. Popov, Covalency versus magnetic axiality in Nd molecular magnets: Nd-photoluminescence, strong ligand-field, and unprecedented nephelauxetic effect in fullerenes $NdM_2N@C_{80}$ (M = Sc, Lu, Y), *Chem. Sci.*, 2024, **15**, 2141–2157.

13 R. Guan, J. Huang, J. Xin, M. Chen, P. Du, Q. Li, Y.-Z. Tan, S. Yang and S.-Y. Xie, A stabilization rule for metal carbido cluster bearing $μ_3$-carbido single-atom-ligand encapsulated in carbon cage, *Nat. Commun.*, 2024, **15**, 150.

14 Y.-R. Yao, J. Zhao, Q. Meng, H.-S. Hu, M. Guo, Y. Yan, J. Zhuang, S. Yang, S. Fortier, L. Echegoyen, W. H. E. Schwarz, J. Li and N. Chen, Synthesis and Characterization of U≡C Triple Bonds in Fullerene Compounds, *J. Am. Chem. Soc.*, 2023, **145**, 25440–25449.

15 Y.-R. Yao, Z.-C. Chen, L. Chen, S.-Y. Zheng, S. Yang, S.-L. Deng, L. Echegoyen, Y.-Z. Tan, S.-Y. Xie and L.-S. Zheng, Two Metastable Endohedral Metallofullerenes $Sc_2C_2@C_1(39656)$-C_{82} and $Sc_2C_2@C_1(51383)$-C_{84}: Direct-C_2-Insertion Products from Their Most Stable Precursors, *J. Am. Chem. Soc.*, 2023, **145**, 16778–16786.

16 H. Jin, J. Xin, W. Xiang, Z. Jiang, X. Han, M. Chen, P. Du, Y.-R. Yao and S. Yang, Bandgap Engineering of Erbium-Metallofullerenes toward Switchable Photoluminescence, *Adv. Mater.*, 2023, **35**, 2304121.

17 H. Jiang, X. Yu, M. Guo, Y.-R. Yao, Q. Meng, L. Echegoyen, J. Autschbach and N. Chen, USc_2C_2 and USc_2NC Clusters with U–C Triple Bond Character Stabilized Inside Fullerene Cages, *J. Am. Chem. Soc.*, 2023, **145**, 5645–5654.

18 C. Huang, R. Sun, L. Bao, X. Tian, C. Pan, M. Li, W. Shen, K. Guo, B. Wang, X. Lu and S. Gao, A hard molecular nano-magnet from confined paramagnetic 3d-4f spins inside a fullerene cage, *Nat. Commun.*, 2023, **14**, 8443.

19 Z. Hu, Y. Wang, A. Ullah, G. M. Gutiérrez-Finol, A. Bedoya-Pinto, P. Gargiani, D. Shi, S. Yang, Z. Shi, A. Gaita-Ariño and E. Coronado, High-temperature magnetic blocking in a monometallic dysprosium azafullerene single-molecule magnet, *Chem*, 2023, **9**, 3613–3622.

20 F. Liu, D. S. Krylov, L. Spree, S. M. Avdoshenko, N. A. Samoylova, M. Rosenkranz, A. Kostanyan, T. Greber, A. U. B. Wolter, B. Büchner and A. A. Popov, Single molecule magnet with an unpaired electron trapped between two lanthanide ions inside a fullerene, *Nat. Commun.*, 2017, **8**, 16098.

21 Y. Maeda, Y. Matsunaga, T. Wakahara, S. Takahashi, T. Tsuchiya, M. O. Ishitsuka, T. Hasegawa, T. Akasaka, M. T. H. Liu, K. Kokura, E. Horn, K. Yoza, T. Kato, S. Okubo, K. Kobayashi, S. Nagase and K. Yamamoto, Isolation and characterization of a carbene derivative of $La@C_{82}$, *J. Am. Chem. Soc.*, 2004, **126**, 6858–6859.

22 T. Akasaka, T. Kono, Y. Takematsu, H. Nikawa, T. Nakahodo, T. Wakahara, M. O. Ishitsuka, T. Tsuchiya, Y. Maeda, M. T. H. Liu, K. Yoza, T. Kato, K. Yamamoto, N. Mizorogi, Z. Slanina and S. Nagase, Does $Gd@C_{82}$ have an anomalous endohedral structure? Synthesis and single crystal X-ray structure of the carbene adduct, *J. Am. Chem. Soc.*, 2008, **130**, 12840–12841.

23 M. Yamada, C. Someya, T. Wakahara, T. Tsuchiya, Y. Maeda, T. Akasaka, K. Yoza, E. Horn, M. T. H. Liu, N. Mizorogi and S. Nagase, Metal atoms collinear with the spiro carbon of 6,6-open adducts, $M_2@C_{80}(Ad)$ (M = La and Ce, Ad = adamantylidene), *J. Am. Chem. Soc.*, 2008, **130**, 1171–1176.

24 X. Lu, Y. Lian, C. M. Beavers, N. Mizorogi, Z. Slanina, S. Nagase and T. Akasaka, Crystallographic X-ray Analyses of $Yb@C_{2v}(3)$-C_{80} Reveal a Feasible Rule That Governs the Location of a Rare Earth Metal inside a Medium-Sized Fullerene, *J. Am. Chem. Soc.*, 2011, **133**, 10772–10775.

25 F. Liu and L. Spree, Molecular spinning top: visualizing the dynamics of $M_3N@C_{80}$ with variable temperature single crystal X-ray diffraction, *Chem. Commun.*, 2019, **55**, 13000–13003.

26 Y. Hao, Y. Wang, L. Spree and F. Liu, Rotation of fullerene molecules in the crystal lattice of fullerene/porphyrin: C_{60} and $Sc_3N@C_{80}$, *Inorg. Chem. Front.*, 2021, **8**, 122–126.

27 Y. Li, T. J. Emge, A. Moreno-Vicente, W. P. Kopcha, Y. Sun, I. F. Mansoor, M. C. Lipke, G. S. Hall, J. M. Poblet, A. Rodríguez-Fortea and J. Zhang, Unexpected Formation of Metallofulleroids from Multicomponent Reactions, with Crystallographic and Computational Studies of the Cluster Motion, *Angew. Chem., Int. Ed.*, 2021, **60**, 25269–25273.

28 Y. Wang and F. Liu, Fullerene rotation dictated by benzene–fullerene interactions, *Inorg. Chem. Front.*, 2024, **11**, 3458–3464.

6348 | *Inorg. Chem. Front.*, 2024, **11**, 6343–6349

This journal is © the Partner Organisations 2024

29 F. Liu, G. Velkos, D. S. Krylov, L. Spree, M. Zalibera, R. Ray, N. A. Samoylova, C.-H. Chen, M. Rosenkranz, S. Schiemenz, F. Ziegs, K. Nenkov, A. Kostanyan, T. Greber, A. U. B. Wolter, M. Richter, B. Büchner, S. M. Avdoshenko and A. A. Popov, Air-stable redox-active nanomagnets with lanthanide spins radical-bridged by a metal–metal bond, *Nat. Commun.*, 2019, **10**, 571.

30 Q. Meng, L. Abella, Y.-R. Yao, D.-C. Sergentu, W. Yang, X. Liu, J. Zhuang, L. Echegoyen, J. Autschbach and N. Chen, A charged diatomic triple-bonded U≡N species trapped in C_{82} fullerene cages, *Nat. Commun.*, 2022, **13**, 7192.

31 S. F. Yang, A. A. Popov and L. Dunsch, Violating the Isolated Pentagon Rule (IPR): The endohedral Non-IPR cage of $Sc_3N@C_{70}$, *Angew. Chem., Int. Ed.*, 2007, **46**, 1256–1259.

32 Y. Hao, Y. Wang, V. Dubrovin, S. M. Avdoshenko, A. A. Popov and F. Liu, Caught in Phase Transition: Snapshot of the Metallofullerene $Sc_3N@C_{70}$ Rotation in the Crystal, *J. Am. Chem. Soc.*, 2021, **143**, 612–616.

33 M. H. Olmstead, A. de Bettencourt-Dias, J. C. Duchamp, S. Stevenson, D. Marciu, H. C. Dorn and A. L. Balch, Isolation and structural characterization of the endohedral fullerene $Sc_3N@C_{78}$, *Angew. Chem., Int. Ed.*, 2001, **40**, 1223–1225.

34 J. M. Campanera, C. Bo, M. M. Olmstead, A. L. Balch and J. M. Poblet, Bonding within the endohedral fullerenes $Sc_3N@C_{78}$ and $Sc_3N@C_{80}$ as determined by density functional calculations and reexamination of the crystal struc-

ture of $\{Sc_3N@C_{78}\}\cdot Co(OEP)\cdot 1.5(C_6H_6)\cdot 0.3(CHCl_3)$, *J. Phys. Chem. A*, 2002, **106**, 12356–12364.

35 B. Q. Mercado, M. N. Chaur, L. Echegoyen, J. A. Gharamaleki, M. M. Olmstead and A. L. Balch, A single crystal X-ray diffraction study of a fully ordered cocrystal of pristine $Sc_3N@D_{3h}(5)–C_{78}$, *Polyhedron*, 2013, **58**, 129–133.

36 M. M. Olmstead, D. A. Costa, K. Maitra, B. C. Noll, S. L. Phillips, P. M. Van Calcar and A. L. Balch, Interaction of curved and flat molecular surfaces. The structures of crystalline compounds composed of fullerene (C_{60}, $C_{60}O$, C_{70}, and $C_{120}O$) and metal octaethylporphyrin units, *J. Am. Chem. Soc.*, 1999, **121**, 7090–7097.

37 U. Mueller, R. Förster, M. Hellmig, F. U. Huschmann, A. Kastner, P. Malecki, S. Pühringer, M. Röwer, K. Sparta, M. Steffien, M. Ühlein, P. Wilk and M. S. Weiss, The macro-molecular crystallography beamlines at BESSY II of the Helmholtz-Zentrum Berlin: Current status and perspectives, *Eur. Phys. J. Plus*, 2015, **130**, 141.

38 W. Kabsch, XDS, *Acta Crystallogr., Sect. D: Biol. Crystallogr.*, 2010, **66**, 125–132.

39 K. M. Sparta, M. Krug, U. Heinemann, U. Mueller and M. S. Weiss, XDSAPP2.0, *J. Appl. Crystallogr.*, 2016, **49**, 1085–1092.

40 G. Sheldrick, Crystal structure refinement with SHELXL, *Acta Crystallogr., Sect. C: Struct. Chem.*, 2015, **71**, 3–8.

41 A. Kostanyan, R. Westerström, Y. Zhang, D. Kunhardt, R. Stania, B. Büchner, A. A. Popov and T. Greber, Switching Molecular Conformation with the Torque on a Single Magnetic Moment, *Phys. Rev. Lett.*, 2017, **119**, 237202.

This journal is © the Partner Organisations 2024

Inorg. Chem. Front., 2024, **11**, 6343–6349 | **6349**